K^0 photoproduction on the deuteron and the extraction of the elementary amplitude

A. Salam* and K. Miyagawa
Simulation Science Center, Okayama University of Science, 1-1 Ridai-cho, Okayama 700-0005, Japan

T. Mart
Departemen Fisika, FMIPA, Universitas Indonesia, Depok 16424, Indonesia

C. Bennhold
Center for Nuclear Studies, Department of Physics, The George Washington University, Washington, DC 20052, USA

W. Glöckle
Institut für Theoretische Physik II, Ruhr-Universität Bochum, D-44780 Bochum, Germany
(Received 21 March 2006; published 26 October 2006)

The photoproduction of K^0 on the deuteron has been investigated with the inclusion of the YN and KN final-state interaction (FSI), as well as the pion-mediated process $\gamma d \to \pi NN \to KYN$. The YN rescattering effects for the inclusive cross section are found to be large in the threshold regions. Polarization observables show sizable FSI effects at larger kaon and hyperon angles. It is shown that the extraction of the elementary $\gamma N \to KY$ amplitude is possible in the quasifree scattering region where FSI effects are negligible. Furthermore, the cross sections in this region are large, indicating that measurements in this kinematic region are favored.

DOI: 10.1103/PhysRevC.74.044004 PACS number(s): 13.60.Le, 13.75.Ev, 13.75.Jz, 25.20.Lj

I. INTRODUCTION

To have a comprehensive understanding of the strong interaction, it is important to learn more about the hyperon-nucleon (YN) interaction. It could be studied through hyperon-nucleon scattering in a straightforward manner, though the lack of hyperon beams makes it difficult experimentally. Instead, kaon photoproduction on the deuteron is a suitable alternative for studying the hyperon-nucleon interaction in the final state. Several previous studies [1–4] have been done of the inclusive and exclusive kaon photoproduction on the deuteron using simple Λn potentials. In a recent calculation, Yamamura *et al.* [5] investigated YN final-state interaction (FSI) effects of the K^+ channels using the more realistic Nijmegen YN potentials [6,7]. They found sizable FSI effects in both exclusive and inclusive cross sections, particularly near the Σ threshold, and concluded that precise data would allow the study of the YN interaction in a great detail. This work was extended in Ref. [8] with the inclusion of kaon-nucleon (KN) rescattering in the final state and the pion-mediated process $\gamma d \to \pi NN \to KYN$ (πN-KY process for short) in the intermediate state. Other recent calculations [9,10] investigating these effects reached similar conclusions.

Regarding kaon photoproduction on the nucleon, the most understood channels are the proton ones [11–16], i.e., $\gamma p \to K^+\Lambda$ and $\gamma p \to K^+\Sigma^0$, since a relatively large number of experimental data are available for these channels [17–19]. Meanwhile, the study of neutron channels is needed to complete our understanding about kaon photoproduction on the nucleon. In these channels, the elementary operator can be quite different. Because of isospin conservation at the hadronic vertices, there is no Λ contribution in the intermediate states of the $\gamma n \to K^+\Sigma^-$ process. Furthermore, in the processes $\gamma n \to K^0\Lambda$ and $\gamma n \to K^0\Sigma^0$, there is no t-channel contribution in the Born terms since K^0 has zero electrical charge. Since free neutron targets are not available to study the neutron channels, one needs to use light nuclei such as the deuteron or ^{3}He as effective neutron targets. The deuteron is particularly well suited because of its small binding energy and its simple structure. Therefore, kaon photoproduction on the deuteron is the natural avenue in the investigation of kaon photoproduction on the neutron.

With the purpose of extracting the elementary cross section on the neutron target, Li *et al.* [20] have calculated the processes $d(\gamma, K^0p)\Lambda$, $d(\gamma, K^0p)\Sigma^0$, and $d(\gamma, K^+p)\Sigma^-$, where the kaon is detected in coincidence with the outgoing nucleon in the impulse approximation (IA). They concluded that within the framework of their model, the deuteron can indeed be used to study K^0 and K^+ photoproduction from the neutron.

Very recently, an experiment of K^0 photoproduction on the deuteron was conducted at the Laboratory of Nuclear Science (LNS) in Sendai [21], in which the cross section of the $d(\gamma, K^0)\Lambda p$ process was measured at a photon energy around 1.1 GeV with forward kaon angles. The data are now being analyzed. In the near future, the same group plans to measure the cross section for the exclusive process and some polarization observables [22]. Similarly, for the same reaction, high-precision data from Jefferson Lab are being analyzed that have become available through the pentaquark searches [23]. In view of these experiments, this paper extends the previous work in [5] by calculating K^0 photoproduction on the deuteron and taking into account the effects of KN rescattering and the πN-KY process. Other rescattering processes (see, for

*Permanent address: Departemen Fisika, FMIPA, Universitas Indonesia, Depok 16424, Indonesia.

example, Fig. 2 in [10]) will not be included in our study, since for the kinematics considered here (close to quasifree scattering or to the YN thresholds) they do not contribute significantly. In extracting the elementary amplitude from the cross section, we only consider the $\gamma d \to K^0 \Lambda p$ channel, since the corresponding measurements have been performed. In Sec. II, we briefly review the production operator used in this work. The formalism for calculating the transition matrix and observables are shown in Sec. III. The results are presented in Sec. IV, and we close the paper with conclusions in Sec. V.

II. THE KAON PHOTOPRODUCTION OPERATOR

Most analyses of kaon photoproduction on the nucleon have been performed at tree level in an effective Lagrangian approach. While this leads to violation of unitarity, this kind of isobar model provides a simple tool to parametrize the elementary process because it is relatively easy to calculate and to use for production on nuclei. In this approach, the photoproduction amplitude $\gamma N \to KY$ (in the following denoted as elementary amplitude) can be written as

$$\langle \vec{p}_Y \mu_Y | t_\lambda^{\gamma K} | \vec{p}_N \mu_N \rangle = \bar{u}_{\mu_Y} \left(\sum_{i=1}^{4} A_i \Gamma_\lambda^i \right) u_{\mu_N}, \qquad (1)$$

where A_i are invariant amplitudes as functions of the Mandelstam variables only. The hyperon and nucleon Dirac spinors are denoted by u_{μ_Y} and u_{μ_N}, respectively. The invariant Dirac operators Γ_λ^i, which are given by

$$\Gamma_\lambda^1 = \tfrac{1}{2}\gamma_5(\not{\epsilon}_\lambda \not{k} - \not{k}\not{\epsilon}_\lambda), \qquad (2)$$

$$\Gamma_\lambda^2 = \gamma_5[(2q-k)\cdot\epsilon_\lambda P\cdot k - (2q-k)\cdot k P\cdot\epsilon_\lambda], \qquad (3)$$

$$\Gamma_\lambda^3 = \gamma_5(q\cdot k\not{\epsilon}_\lambda - q\cdot\epsilon_\lambda \not{k}), \qquad (4)$$

$$\Gamma_\lambda^4 = i\epsilon_{\mu\nu\rho\sigma}\gamma^\mu q^\nu \epsilon_\lambda^\rho k^\sigma, \qquad (5)$$

are gauge-invariant Lorentz pseudoscalars and given in terms of the usual γ matrices, the photon momentum k, and its polarization vector ϵ_λ. Here, λ labels the polarization states, q is the meson momentum, and $P = (p' + p)/2$, where p and p' denote initial and final baryon momenta, respectively [24]. By expressing the Dirac operators and spinors in term of Pauli matrices $\vec{\sigma}$ and spinors χ, we can write the kaon photoproduction operator as

$$t_\lambda^{\gamma K} = i(L_\lambda + i\vec{\sigma}\cdot\vec{K}_\lambda), \qquad (6)$$

where L_λ and $\vec{K}_\lambda$ are functions of A_i. The rather lengthy expression of A_i, L_λ, and $\vec{K}_\lambda$ can be found in Ref. [12].

In the present work we use the KAON-MAID model [14], which includes the $D_{13}(1895)$ resonance besides the Born terms and other resonances. Separate hadronic form factors for each vertex were used. To restore gauge invariance, the recipe from Haberzettl [25] was utilized. The coupling constants and cutoff parameters were determined by fitting to the experimental data. The behavior of this model in all six isospin channels is exhibited by the dashed lines in Fig. 1.

Recently, the SAPHIR Collaboration at the Electron Stretcher Accelerator (ELSA) in Bonn published new data on all proton channels, i.e., the $\gamma p \to K^+\Lambda$, $\gamma p \to K^+\Sigma^0$, and $\gamma p \to K^0\Sigma^+$ ones. The new data are more precise and cover all angular distributions in the energy range from threshold up to $W \simeq 2.4$ GeV. Furthermore, as shown by the middle- and lower-left panels of Fig. 1, these new data show a significant discrepancy with data from the previous experiment in the $\gamma p \to K^+\Sigma^0$ and $\gamma p \to K^0\Sigma^+$ channels. Since KAON-MAID was fitted to previous data, it obviously faces a problem in reproducing the new ones. Figure 1 reveals this problem explicitly.

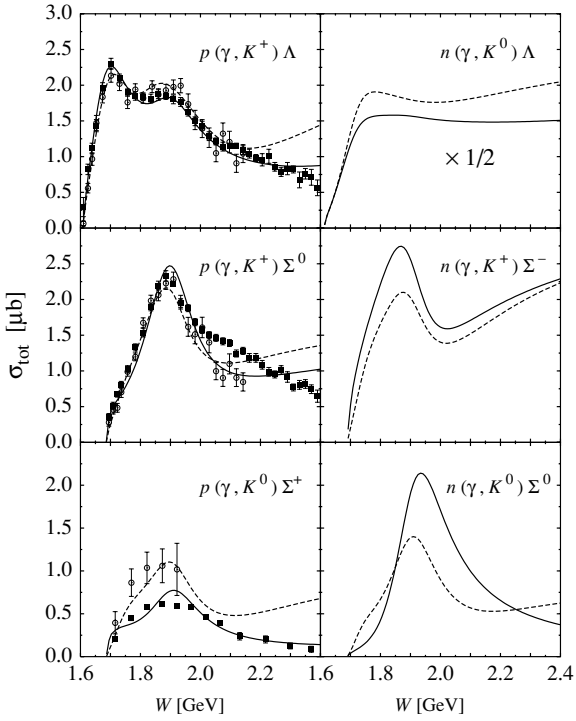

FIG. 1. Total cross section of kaon photoproduction on the nucleon obtained by using the original KAON-MAID model (dashed lines) and the same model but refitted to the new SAPHIR data (solid lines). Older experimental data are taken from Refs. [18,19]; new SAPHIR data are from [26,27].

To investigate the effects of the new data on KAON-MAID, we refitted the coupling constants in this isobar model by only using the new SAPHIR data in our database. The results are shown by the solid lines in Fig. 1. While in the $\gamma p \to K^+\Lambda$ and $\gamma p \to K^0\Sigma^+$ channels KAON-MAID can nicely reproduce the new measurements, it is obviously unable to explain the $\gamma p \to K^+\Sigma^0$ cross section at $W \gtrsim 2.0$ GeV, because KAON-MAID does not have certain resonances at this energy region. By floating the resonance masses during the fit process, a recent study has shown that the new data on this channel demand a nucleon resonance S_{11} with $M \simeq 2.1$ GeV [27].

The predicted total cross sections for neutron channels are given in the three right panels of Fig. 1. There are sizable differences between the original prediction of KAON-MAID and the refitted version. Nevertheless, all predicted cross sections are of the same order.

Very recently, the CLAS Collaboration has also published its data for both $\gamma p \to K^+\Lambda$ and $\gamma p \to K^+\Sigma^0$ channels [28,29]. The CLAS data show, unfortunately, substantial and

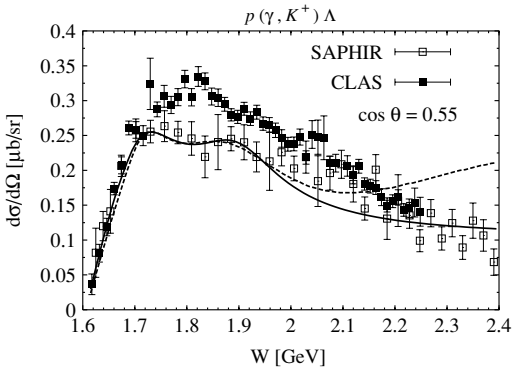

FIG. 2. Example of the systematic discrepancy between SAPHIR (open squares) [27] and CLAS (solid squares) [28] data in the differential cross section of the $\gamma p \to K^+\Lambda$ channel as a function of the total c.m. energy W. Predictions from the two elementary operator models given in Fig. 1 are shown for comparison.

systematic discrepancies with the SAPHIR ones. This problem is clearly illustrated in Fig. 2. As a consequence, an effort to simultaneously fit the model to both data versions would be meaningless. In view of this, we decided to use the original KAON-MAID model in the subsequent calculations. This choice is also supported by the fact that in this paper most calculations on the deuteron have been performed at low photon energy, a region where the original and the refitted KAON-MAID models are still in good agreement and the discrepancy in the new experimental data is not too significant. Furthermore, our main motivation in this paper is to show the possibility of extracting the elementary cross section for the $\gamma N \to KY$ process from the deuteron cross section. Therefore, we can expect that the main conclusion will be independent from the choice of elementary model.

III. THE REACTION ON THE DEUTERON

A. Cross sections and amplitudes

The general expression for the cross section using the convention of Bjorken and Drell [30] is given by

$$d\sigma = \frac{1}{|\vec{v}_\gamma - \vec{v}_d|}\frac{m_Y m_N}{8E_\gamma E_K E_d E_Y E_N}\frac{d\vec{p}_K}{(2\pi)^3}\frac{d\vec{p}_Y}{(2\pi)^3}\frac{d\vec{p}_N}{(2\pi)^3}(2\pi)^4 \times \delta^4(P_d + Q - p_Y - p_N)\frac{1}{6} \times \sum_{\mu_Y\mu_N\mu_d\lambda} \left|\sqrt{2}\langle \vec{p}_Y\vec{p}_N\mu_Y\mu_N|T_\lambda^{\gamma K}|\Psi_{\mu_d}\rangle\right|^2, \quad (7)$$

where μ_Y, μ_N, μ_d, and λ denote the spin projections of hyperon, nucleon, and deuteron and the photon polarization, respectively. For the deuteron state Ψ_{μ_d}, however, we use a noncovariant notation, which removes the standard additional factor $1/2E_d(2\pi)^3$. Here, $Q = p_\gamma - p_K$ is the momentum transfer to the two-baryon system, and the factor $\sqrt{2}$ comes from the proper antisymmetrization. In this expression, the dependencies on the kinematic variables have been suppressed, and it should be understood that the production operator acts on one of the two initial baryons. By integrating the right hand side of Eq. (7) over the three-momentum of nucleon and momentum of hyperon, followed by rewriting the flux factor, we arrive at the cross section for the exclusive process $d(\gamma, KY)N$ in the deuteron rest frame, i.e.,

$$\frac{d\sigma}{dp_K d\Omega_K d\Omega_Y} = \frac{m_Y m_N |\vec{p}_K|^2|\vec{p}_Y|^2}{4(2\pi)^2 E_\gamma E_K} - |(E_Y + E_N)|\vec{p}_Y|E_Y\vec{Q}\cdot\hat{p}_Y|^{-1}\frac{1}{6} \times \sum_{\mu_Y\mu_N\mu_d\lambda} \left|\sqrt{2}\langle \vec{p}_Y\vec{p}_N\mu_Y\mu_N|T_\lambda^{\gamma K}|\Psi_{\mu_d}\rangle\right|^2. \quad (8)$$

Throughout the paper, we work in the deuteron rest frame. For the inclusive process $d(\gamma, K)YN$, the cross section is given by

$$\frac{d\sigma}{dp_K d\Omega_K} = \int d\Omega_Y^{\text{c.m.}}\frac{m_Y m_N |\vec{p}_K|^2|\vec{p}_Y^{\text{c.m.}}|}{4(2\pi)^2 E_\gamma E_K W} \times \frac{1}{6}\sum_{\mu_Y\mu_N\mu_d\lambda} \left|\sqrt{2}\langle \vec{p}_Y\vec{p}_N\mu_Y\mu_N|T_\lambda^{\gamma K}|\Psi_{\mu_d}\rangle\right|^2, \quad (9)$$

where $W^2 = (P_d + Q)^2$ and $|\vec{p}_Y^{\text{c.m.}}|$ is the hyperon momentum calculated in the center-of-mass frame of the two final baryons.

The amplitude is approximated by the diagram shown in Fig. 3, which is written for convenience as

$$T_\lambda^{\gamma K} = t^{\gamma K} + t_{YN}^{\gamma K} + t_{KN}^{\gamma K} + t_{K\pi}^{\gamma K}, \quad (10)$$

where $t^{\gamma K}, t_{YN}^{\gamma K}, t_{KN}^{\gamma K}$, and $t_{K\pi}^{\gamma K}$ denote the operators for the impulse approximation (IA) hyperon-nucleon rescattering, kaon-nucleon rescattering, and the pion mediated process, respectively.

The IA and YN rescattering terms are calculated precisely. Here, we describe the calculation briefly; the reader should consult Ref. [5] for details. The operator of the sum of diagrams

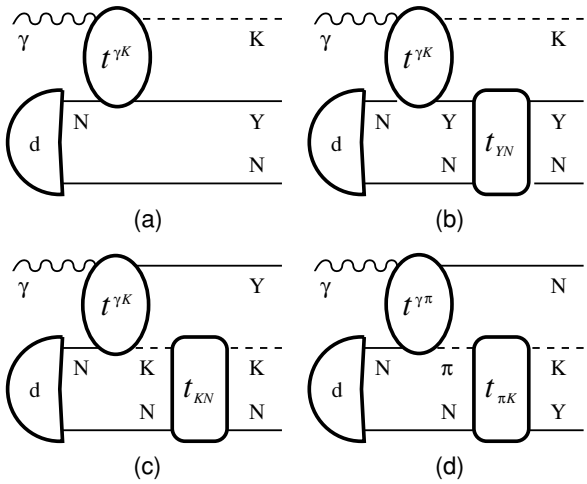

FIG. 3. Kaon photoproduction on the deuteron. (a) impulse approximation (IA), (b) YN rescattering, (c) KN rescattering, and (d) πN-KY process.

(a) and (b) can be written as

$$T_{YN}^{\gamma K} = t^{\gamma K} + t_{YN}^{\gamma K}, \tag{11}$$

$$= t^{\gamma K} + t_{YN} G_{YN} t^{\gamma K}, \tag{12}$$

with the YN scattering operator t_{YN} which obeys the Lippmann-Schwinger equation

$$t_{YN} = V_{YN} + V_{YN} G_{YN} t_{YN}\,, \tag{13}$$

where V_{YN} denotes the YN potential operator and G_{YN} the free YN propagator. Inserting Eq. (13) into Eq. (12), we obtain

$$T_{YN}^{\gamma K} = t^{\gamma K} + V_{YN} G_{YN} T_{YN}^{\gamma K}\,, \tag{14}$$

which can be solved by inversion, i.e.,

$$T_{YN}^{\gamma K} = (1 - V_{YN} G_{YN})^{-1} t^{\gamma K}\,. \tag{15}$$

After solving the last equation in a partial-wave decomposition with respect to the YN subsystem, one obtains the YN rescattering amplitude by subtracting the IA term.

The KN rescattering [diagram (c) in Fig. 3] is evaluated directly in contrast to YN rescattering. The corresponding operator is given by

$$t_{KN}^{\gamma K} = t_{KN} G_{KN} t^{\gamma K}\,, \tag{16}$$

where t_{KN} is the KN scattering operator, which also obeys the Lippmann-Schwinger equation of the form (13), and G_{KN} is the free KN propagator. For V_{KN}, we take a rank-1 separable potential which, in the partial-wave representation, is given by

$$V_{\ell J}(p', p) = \lambda_{\ell J} g(p')_{\ell J}\, g(p)_{\ell J}, \tag{17}$$

with the form factor

$$g(p)_{\ell J} = \frac{B_{\ell J} p^{\ell}}{\left[p^2 + A_{\ell J}^2\right]^{\frac{\ell+2}{2}}}\,, \tag{18}$$

where $\lambda_{\ell J}$, $B_{\ell J}$, and $A_{\ell J}$ are parameters which are determined by fitting the phase shift to the experimental data [31,32]. The πN-KY process [diagram (d) in Fig. 3] is calculated in the same fashion; details of these calculations can be found in Ref. [8].

B. Polarization observables

With respect to polarization observables, we consider the tensor target asymmetries T_{2M} which are given by [33]

$$T_{2M} \frac{d\sigma}{d\Omega_K} = (2 - \delta_{M0})\, \mathcal{R}e V_{2M}\,, \quad M = 0, 1, 2\,, \tag{19}$$

where

$$V_{2M} = \sqrt{15} \sum_{\mu_Y \mu_N \lambda} \sum_{\mu_d' \mu_d} (-1)^{1-\mu_d'} \begin{pmatrix} 1 & 1 & 2 \\ \mu_d & -\mu_d' & -M \end{pmatrix} \times \int_{p_K^{\min}}^{p_K^{\max}} dp_K \int d\Omega_Y^{\text{c.m.}}\, \kappa \mathcal{M}^*_{\mu_Y \mu_N \mu_d \lambda} \mathcal{M}_{\mu_Y \mu_N \mu_d' \lambda} \tag{20}$$

with a kinematic factor

$$\kappa = \frac{m_Y m_N |\vec{p}_K|^2 \left|\vec{p}_Y^{\,\text{c.m.}}\right|}{24(2\pi)^2 E_\gamma E_K W}\,. \tag{21}$$

We also calculate the hyperon recoil polarization P_y, the beam asymmetry Σ, and the double polarization C_x and C_z, which are given by

$$P_y = \frac{\mathrm{Tr}\, \mathcal{M} \mathcal{M}^+ \sigma_y}{\mathrm{Tr}\, \mathcal{M} \mathcal{M}^+}\,, \tag{22}$$

$$\Sigma = \frac{\mathrm{Tr}\, \mathcal{M}_{\epsilon_y} \mathcal{M}_{\epsilon_y}^+ - \mathrm{Tr}\, \mathcal{M}_{\epsilon_x} \mathcal{M}_{\epsilon_x}^+}{\mathrm{Tr}\, \mathcal{M}_{\epsilon_y} \mathcal{M}_{\epsilon_y}^+ + \mathrm{Tr}\, \mathcal{M}_{\epsilon_x} \mathcal{M}_{\epsilon_x}^+}\,, \tag{23}$$

$$C_x = \frac{\mathrm{Tr}\, \mathcal{M}_{\epsilon_1} \mathcal{M}_{\epsilon_1}^+ \sigma_x}{\mathrm{Tr}\, \mathcal{M}_{\epsilon_1} \mathcal{M}_{\epsilon_1}}\,, \tag{24}$$

$$C_z = \frac{\mathrm{Tr}\, \mathcal{M}_{\epsilon_1} \mathcal{M}_{\epsilon_1}^+ \sigma_z}{\mathrm{Tr}\, \mathcal{M}_{\epsilon_1} \mathcal{M}_{\epsilon_1}}\,. \tag{25}$$

In these equations, amplitude $\mathcal{M}$ reads

$$\mathcal{M} = \sqrt{2}\, \langle \vec{p}_Y \vec{p}_N \mu_Y \mu_N | T_\lambda^{\gamma K} | \Psi_{\mu_d} \rangle, \tag{26}$$

where, for example, $\mathcal{M}_{\epsilon_y}$ indicates the amplitude with photon polarization pointing into the y axis, i.e., $\vec{\epsilon}_\lambda = \vec{\epsilon}_y$. The photon polarization $\vec{\epsilon}_1 = -\frac{1}{\sqrt{2}}(\vec{\epsilon}_x + i\vec{\epsilon}_y)$ describes the helicity state $+1$. The beam asymmetry Σ is obtained with linearly polarized photon, while the double polarization observables C_x and C_z are the observables for both polarized hyperon and circularly polarized photon.

C. Extraction of the elementary amplitude

In the following, we describe briefly the extraction of the invariant elementary amplitude from the cross section on the deuteron in view of the study of kaon photoproduction on the neutron. The condition for the extraction must be that FSI effects are negligible. Thus, the amplitude can be approximated only by the impulse term. In this case, the invariant elementary amplitude can be separated from the deuteron one. To show this, first we write the amplitude of the impulse term explicitly as

$$\langle \vec{p}_Y \vec{p}_N \mu_Y \mu_N | t_\lambda^{\gamma K} | \Psi_{\mu_d} \rangle = \sum_{\mu_{N'}} \langle \vec{p}_Y \mu_Y | t_\lambda^{\gamma K} | -\vec{p}_N \mu_{N'} \rangle \times C^{\frac{1}{2}\,\frac{1}{2}\,1}_{\mu_N \mu_{N'} \mu_S} \Psi_{\mu_S \mu_d}(-\vec{p}_N), \tag{27}$$

where C denotes the Clebsch-Gordan coefficient and $\vec{p}_N$ is the spectator nucleon momentum. The deuteron wave function Ψ is given by

$$\Psi_{\mu_S \mu_d}(-\vec{p}_N) = \sum_\ell C^{\ell\,1\,1}_{\mu_\ell \mu_S \mu_d} u_\ell(|\vec{p}_N|) Y_{\ell \mu_\ell}(-\hat{p}_N), \tag{28}$$

where Y indicates spherical harmonics and u is its radial part, which is generated by the Nijmegen93 NN potential [34] in this work. Summing over all spin states of the amplitude in Eq. (27), after some algebra we find

$$\sum_{\mu_Y \mu_N \mu_d \lambda} \left| \langle \vec{p}_Y \vec{p}_N \mu_Y \mu_N | t_\lambda^{\gamma K} | \Psi_{\mu_d} \rangle \right|^2 = D \sum_{\mu_Y \mu_{N'} \lambda} \left| \langle \vec{p}_Y \mu_Y | t_\lambda^{\gamma K} | -\vec{p}_N \mu_{N'} \rangle \right|^2, \tag{29}$$

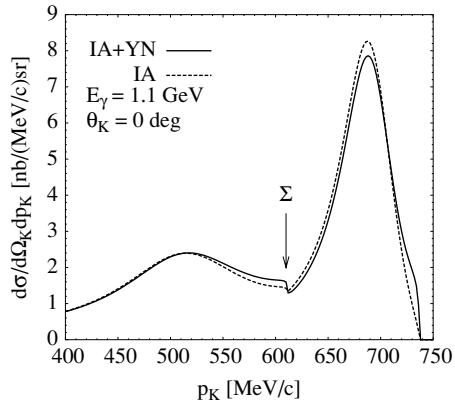

FIG. 4. Inclusive cross sections of $d(\gamma, K^0)YN$ as functions of p_K at $E_\gamma = 1.1$ GeV and $\theta_K = 0^\circ$. Dashed line denotes the IA results; solid line, the IA + YN results. Arrow indicates the Σ threshold.

where

$$D = \tfrac{3}{2}|Y_{00}|^2 u_0^2 + \left(\tfrac{3}{10}|Y_{20}|^2 + \tfrac{3}{5}|Y_{21}|^2 + \tfrac{3}{5}|Y_{22}|^2\right)u_2^2. \quad (30)$$

With this expression we can write Eq. (8) as

$$\frac{d\sigma}{dp_K d\Omega_K d\Omega_Y} = \frac{m_Y m_N |\vec{p}_K|^2 |\vec{p}_Y|^2}{4(2\pi)^2 E_\gamma E_K} - |(E_Y + E_N)|\vec{p}_Y| E_Y \vec{Q}\cdot\hat{p}_Y|^{-1}\frac{1}{6}D - \sum_{\mu_Y \mu_{N'} \lambda} \left|\langle \vec{p}_Y \mu_Y | t_\lambda^{\gamma K} | \vec{p}_N \mu_{N'}\rangle\right|^2. \quad (31)$$

On the right hand side of this equation, the sum of the squared amplitudes of the elementary process $\gamma N \to KY$ has been completely separated from the deuteron wave function.

IV. RESULTS

The inclusive cross section, calculated using Eq. (9) at a photon energy of $E_\gamma = 1.1$ GeV and at forward kaon angle $\theta_K = 0^\circ$, is shown in Fig. 4. In this figure, we add up the cross sections for all outgoing channels, $K^0\Lambda p$, $K^0\Sigma^0 p$, and $K^0\Sigma^+ n$. The positions of the two peaks are found to be consistent with the Λ and Σ quasifree scattering (QFS) conditions. We note sizable effects of YN rescattering in the Λ and Σ threshold regions and on the top of the Λ peak around $p_K = 690$ MeV/c. Figure 5 shows the inclusive cross sections in IA, where the results for the two different elementary operators discussed in Sec. II are compared. This figure shows a relatively large variation of the cross sections around the Σ-QFS region. This result originates from the different models for the elementary process (see Fig. 1) of the $K^+\Sigma^-$ channel at this energy of $W \simeq 1.7$ GeV. The other $K\Sigma$ channels also exhibit significant differences, but since their overall cross

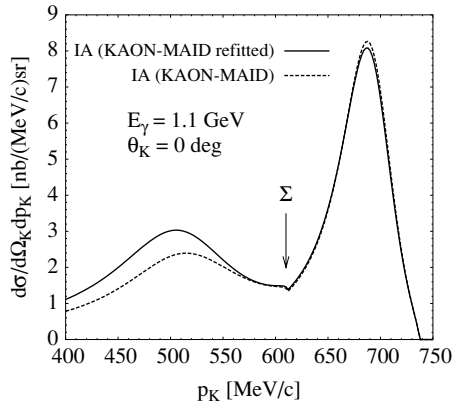

FIG. 5. Comparison of the inclusive cross sections in IA using the two different elementary models given in Fig 1.

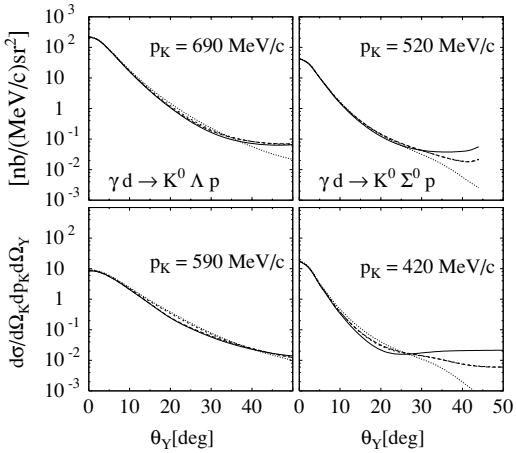

FIG. 6. Exclusive cross sections as a function of hyperon angle θ_Y for $\gamma d \to K^0\Lambda p$ (left panels) and $\gamma d \to K^0\Sigma^0 p$ (right panels) at the photon energy $E_\gamma = 1.1$ GeV, kaon angle $\theta_K = 0^\circ$, hyperon angle $\phi_Y = 0^\circ$ for two values of the kaon momentum $\vec{p}_K$. Dotted line corresponds to IA, short-dashed line to IA+YN, dashed line to IA + YN + KN, and solid line to IA + YN + $KN(+\pi N$-$KY)$.

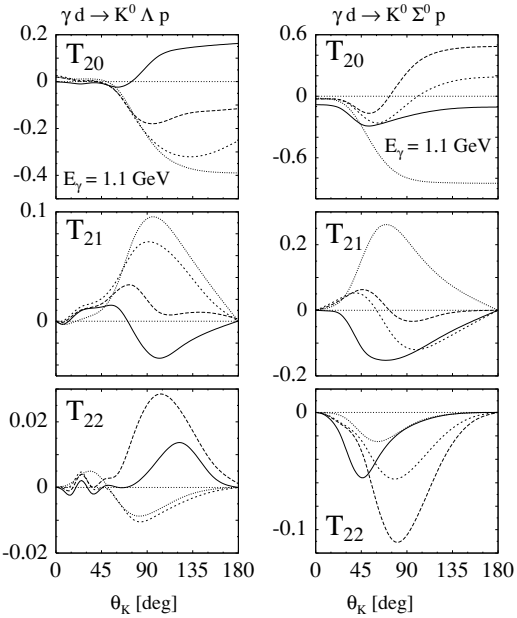

FIG. 7. Tensor asymmetries T_{20}, T_{21}, and T_{22}, as functions of kaon angle θ_K for $\gamma d \to K^0\Lambda p$ (left panels) and $\gamma d \to K^0\Sigma^0 p$ (right panels) for $E_\gamma = 1.1$ GeV. Lines are as in Fig. 6.

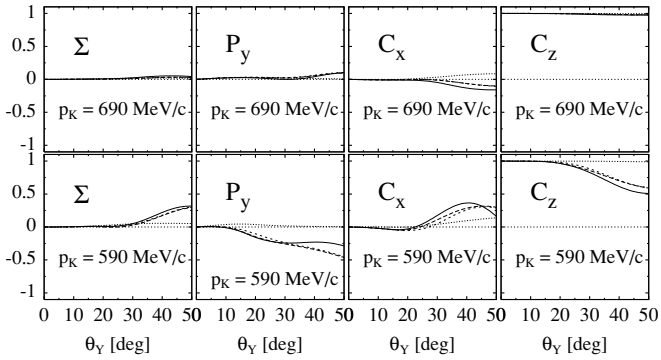

FIG. 8. Beam asymmetry Σ, recoil polarization P_y, and double polarizations C_x and C_z for the $\gamma d \to K^0 \Lambda p$ process, as functions of the hyperon angle θ_Y for two kaon momenta p_K. $E_\gamma = 1.1$ GeV, $\theta_K = 0^\circ$, and $\phi_Y = 0^\circ$. Lines are as in Fig. 6.

sections are smaller compared to $K^+\Sigma^-$, their effects become less important. In contrast to the $K^+\Sigma^-$ channel, for both the $K^+\Lambda$ and $K^0\Lambda$ channels the corresponding cross sections do not differ too much around $W = 1.7$ GeV. This also explains why the difference between the two elementary models does not show up strongly around the Λ-QFS region.

By comparing Figs. 4 and 5, we can see that the variation originating from the different elementary operators is larger than that originating from the FSI effects around the Σ-QFS region. In other words, we can say that the cross section of the process $d(\gamma, K^0)\Sigma N$ is more sensitive to the choice of the elementary operators than to the FSI effects. This feature indicates that the process $d(\gamma, K^0)\Sigma N$ can serve as a way to access the elementary operators. Experimental data with error bars smaller than these variations are needed now to apply our procedure.

Figure 6 presents the exclusive cross sections calculated for the photon energy 1.1 GeV at forward kaon angle $\theta_K = 0^\circ$. The figure shows that the effect of the YN rescattering is stronger at larger hyperon angles, while the effects of KN rescattering and πN-KY process are negligible or small.

The tensor asymmetries for the photon energy of $E_\gamma = 1.1$ GeV are shown in Fig. 7. We see that the YN, KN rescatterings, and πN-KY process have different effects on T_{20}, T_{21}, and T_{22} at larger kaon angles. Figures 8 and

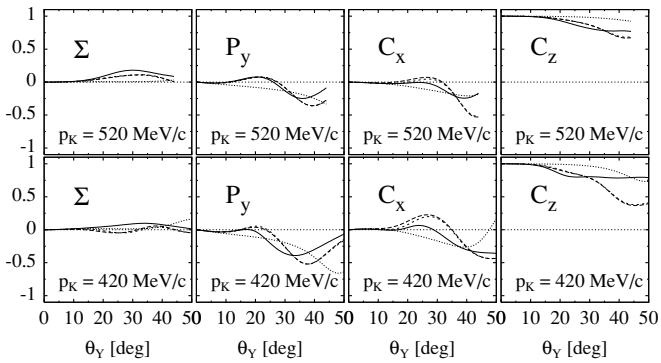

FIG. 9. Same as Fig. 8, but for $\gamma d \to K^0\Sigma^0 p$ with $p_K = 520$ and 420 MeV/c.

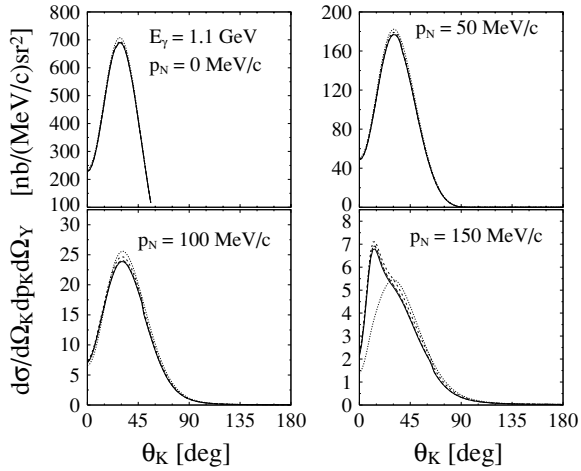

FIG. 10. Exclusive cross sections of $d(\gamma, K^0\Lambda)p$ as functions of kaon angle θ_K for $E_\gamma = 1.1$ GeV. Direction of the outgoing nucleon momentum $\vec{p}_N$ is fixed at $\theta_N = 30^\circ$ and $\phi_N = 180^\circ$, but the magnitude of $\vec{p}_N$ is varied. Results for $p_N = 0$, 50, 100, and 150 MeV/c are shown. Lines are as in Fig. 6.

9 show the polarization observables Σ, P_y, C_x, and C_z in the $\gamma d \to K^0\Lambda p$ and $\gamma d \to K^0\Sigma^0 p$ channels, respectively. These polarization observables are calculated for the photon energy $E_\gamma = 1.1$ GeV, the kaon angle $\theta_K = 0^\circ$, and the hyperon angle $\phi_Y = 0^\circ$. The top panels correspond to the results at the peak positions of the inclusive cross section, while the bottom panels refer to lower kaon momenta. For these observables, the YN rescattering effects dominate at larger hyperon angles θ_Y. The effects are more remarkable at lower kaon momenta than at the peak positions.

Figures 10 and 11 show the exclusive cross sections of $d(\gamma, K^0\Lambda)p$ as a function of kaon angle θ_K for $E_\gamma = 1.1$ and 1.3 GeV, respectively. In the figures, we fix the direction of the outgoing nucleon momentum $\vec{p}_N$ to $\theta_N = 30^\circ$ and $\phi_N = 180^\circ$, while several magnitudes of $\vec{p}_N$, namely, 0, 50, 100, and 150 MeV/c, are studied. At nucleon momentum $p_N = 150$ MeV/c, the effects of YN rescattering are most prominent at forward kaon angles, but almost negligible for zero nucleon

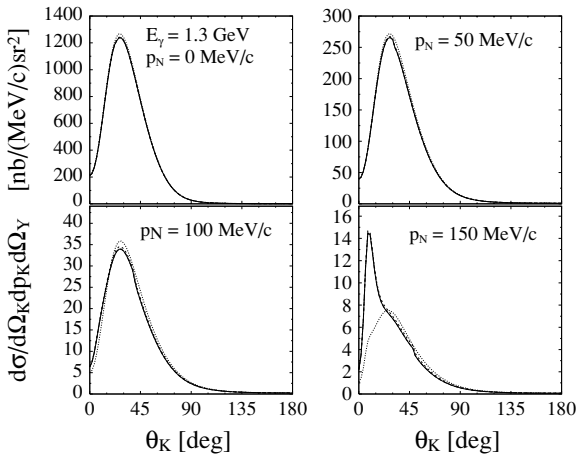

FIG. 11. Same as Fig. 10, but for $E_\gamma = 1.3$ GeV.

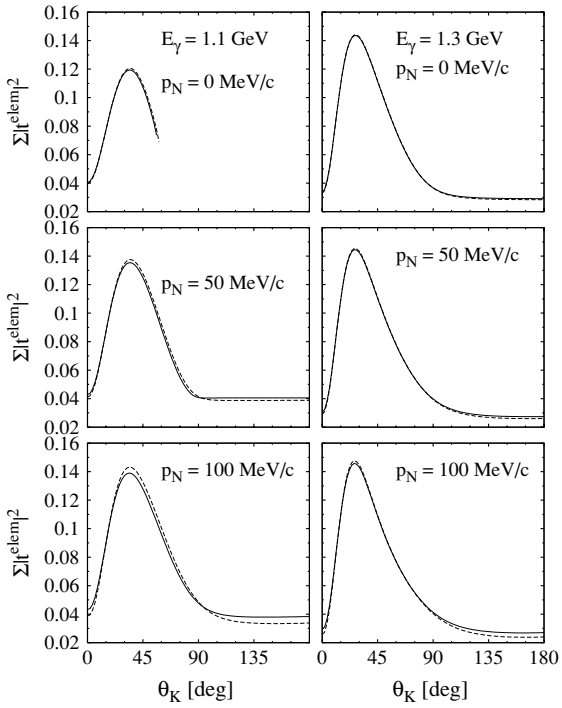

FIG. 12. Comparison between the extracted and the free-process amplitudes squared for $\gamma n \to K^0\Lambda$ at E_γ = 1.1 and 1.3 GeV. Solid line refers to the extracted amplitudes from $\gamma d \to K^0\Lambda p$; dashed line is obtained from the free-process amplitudes. Direction of $\vec{p}_N$ is fixed at $\theta_N = 30^\circ$ and $\phi_N = 180^\circ$, but magnitude of $\vec{p}_N$ is varied with 0, 50, 100 MeV/c.

momentum, i.e., under QFS kinematics. From these features we conclude that the extraction of the elementary amplitude is favored in QFS kinematics.

Finally, in Fig. 12 we compare the extracted elementary amplitudes for $p_N = 0$, 50, and 100 MeV/c with the corresponding free-process amplitudes. We see that the extracted amplitudes are in good agreement with the free-process amplitudes at QFS kinematics. At $p_N = 50$ MeV/c, a small discrepancy is seen between the extracted and the free-process amplitudes, especially at larger kaon angles. The discrepancy

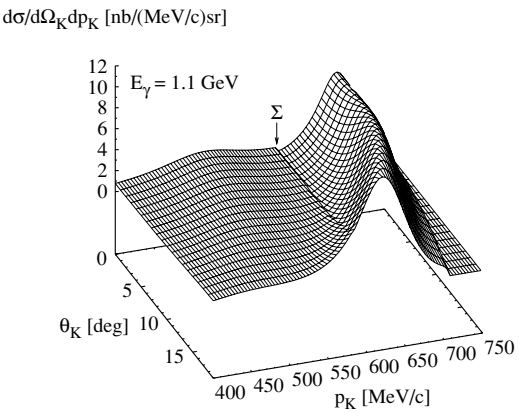

FIG. 13. Three-dimensional plot of $d(\gamma, K^0)YN$ as a function of θ_K and p_K, which is obtained with IA + YN. E_γ = 1.1 GeV.

grows at $p_N = 100$ MeV/c. One can also note from the figures that the extraction works better at higher photon energies E_γ, where the discrepancy is smaller for the same nucleon momentum p_N.

Another feature visible in Figs. 10 and 11 is that the cross section of the exclusive process $d(\gamma, K^0\Lambda)p$ in QFS kinematics is much larger than that in other kinematic regions, indicating that measurements in this region will be easier. For visualizing the QFS regions over a wide range of p_K and θ_K, we provide a three-dimensional plot of the inclusive process $d(\gamma, K^0)\Lambda p$ obtained with IA+YN in Fig. 13, for E_γ = 1.1 GeV. This figure shows a ridge running along the QFS condition which moves to smaller kaon momentum p_K as the kaon angle θ_K increases.

V. SUMMARY AND CONCLUSION

We have analyzed K^0 photoproduction on the deuteron $\gamma d \to KYN$, investigating the effects of YN and KN rescattering and the intermediate πN-KY rescattering process. YN rescattering effects are found to be large in the threshold regions in the inclusive cross section for the forward kaon angle $\theta_K = 0^\circ$. The two models of KAON-MAID for the elementary operator, the original and the one refitted to the new SAPHIR data, show a large variation in the Σ QFS region of the inclusive cross sections. Therefore, the $d(\gamma, K^0)YN$ experiments can serve as a method to access those operators. In the exclusive processes, the polarization observables show visible effects of the final-state interactions at larger hyperon angles.

We have also calculated the exclusive cross section for outgoing nucleon momenta $\vec{p}_N$ with various magnitudes in a fixed direction. The YN rescattering effects are found to become larger at forward kaon angles as the magnitude of $\vec{p}_N$ increases, but those effects are almost negligible at zero nucleon momentum, i.e., under QFS kinematics. We have shown that the elementary amplitude can be extracted algebraically from the full amplitude using the impulse approximation when FSI effects do not contribute. We have performed the extraction for the $\vec{p}_N$ values mentioned above, and the extracted elementary amplitudes have been compared with the free-process ones. At QFS kinematics, the extracted and the free-process amplitudes agree well. This demonstrates that kaon photoproduction on the deuteron in the QFS region is suitable for investigating the elementary process in the neutron channels. The exclusive cross sections for the $d(\gamma, K^0\Lambda)p$ process at the QFS kinematics are found to be especially large, suggesting that this region is appropriate for measurements. We confirm that the region where the cross sections are large develops close to QFS kinematics and forms a ridge on the θ_K-p_K plane.

ACKNOWLEDGMENTS

A.S. would like to thank the Simulation Science Center, Okayama University of Science, Okayama, for financial support and for the very kind hospitality during his stay. This work was supported by the Academic Frontier Project for Private Universities: a matching fund subsidy from MEXT (Ministry of Education, Culture, Sports, Science and Technology), Japan.

[1] F. M. Renard and Y. Renard, Nucl. Phys. **B1**, 389 (1967).
[2] F. M. Renard and Y. Renard, Phys. Lett. **B24**, 159 (1967).
[3] R. A. Adelseck and L. E. Wright, Phys. Rev. C **39**, 580 (1989).
[4] X. Li and L. E. Wright, J. Phys. G: Nucl. Part. Phys. **17**, 1127 (1991).
[5] H. Yamamura, K. Miyagawa, T. Mart, C. Bennhold, W. Glöckle, and H. Haberzettl, Phys. Rev. C **61**, 014001 (1999).
[6] P. M. M. Maessen, Th. A. Rijken, and J. J. de Swart, Phys. Rev. C **40**, 2226 (1989).
[7] Th. A. Rijken, V. G. J. Stoks, and Y. Yamamoto, Phys. Rev. C **59**, 21 (1999).
[8] A. Salam and H. Arenhövel, Phys. Rev. C **70**, 044008 (2004); A. Salam, Dissertation, Johannes Gutenberg Universität, Mainz, 2003 (unpublished).
[9] B. O. Kerbikov, Phys. At. Nucl. **64**, 1835 (2001).
[10] O. V. Maxwell, Phys. Rev. C **69**, 034605 (2004).
[11] J. C. David, C. Fayard, G. H. Lamot, and B. Saghai, Phys. Rev. C **53**, 2613 (1996).
[12] T. Mart, Dissertation, Johannes Gutenberg Universität, Mainz, 1996 (unpublished).
[13] C. Bennhold, T. Mart, and D. Kusno, in Proceedings of the CEBAF/INT Workshop on N^* Physics, Seattle USA, 1996 (unpublished).
[14] T. Mart and C. Bennhold, Phys. Rev. C **61**, 012201(R) (1999); T. Mart, *ibid*. **62**, 038201 (2000).
[15] B. S. Han, M. K. Cheoun, K. S. Kim, and I. T. Cheon, Nucl. Phys. **A691**, 713 (2001).
[16] S. Janssen, J. Ryckebusch, D. Debruyne, and T. Van Cauteren, Phys. Rev. C **65**, 015201 (2002).
[17] M. Bockhorst *et al*., Z. Phys. C **63**, 37 (1994).
[18] M. Q. Tran *et al*., Phys. Lett. **B445**, 20 (1998).
[19] S. Goers *et al*., Phys. Lett. **B464**, 331 (1999).
[20] X. Li, L. E. Wright, and C. Bennhold, Phys. Rev. C **45**, 2011 (1992).
[21] O. Hashimoto (private communication).
[22] K. Maeda (private communication).
[23] P. Nadel-Turonski (private communication).
[24] A. Donnachie, *High Energy Physics* (Academic, New York, 1972), Vol. 5.
[25] H. Haberzettl, Phys. Rev. C **56**, 2041 (1997).
[26] K.-H. Glander *et al*., Eur. Phys. J. A **19**, 251 (2004).
[27] R. Lawall *et al*., Eur. Phys. J. A **24**, 275 (2005).
[28] J. W. C. McNabb *et al*. (CLAS Collaboration), Phys. Rev. C **69**, 042201 (2004).
[29] R. Bradford *et al*. (CLAS Collaboration), Phys. Rev. C **73**, 035202 (2006).
[30] J. D. Bjorken and S. D. Drell, *Relativistic Quantum Mechanics* (McGraw-Hill, New York, 1964).
[31] J. S. Hyslop, R. A. Arndt, L. D. Roper, and R. L. Workman, Phys. Rev. D **46**, 961 (1992).
[32] D. H. Saxon *et al*., Nucl. Phys. **B162**, 522 (1980).
[33] H. Arenhövel, Few-Body Syst. **4**, 55 (1988).
[34] V. G. J. Stoks, R. A. M. Klomp, C. P. F. Terheggen, and J. J. de Swart, Phys. Rev. C **49**, 2950 (1994).